Chinese Chemical Letters 37 (2026) 112344

Contents lists available at ScienceDirect

Chinese Chemical Letters

journal homepage: www.elsevier.com/locate/cclet

Catalytic synthesis of quinones and visual intelligent portable colorimetric detection of phenols by a [Ag-$AlMo_6$]-nanosheet-based hybrid

Lian Yang[a], Guo-Cheng Liu[a,b,*], Na Xu[a], Zhong Zhang[a,c,*], Xiu-Li Wang[a], Yong-Ge Wei[b,*]

[a] College of Chemistry, Bohai University, Jinzhou 121013, China
[b] Key Lab of Organic Optoelectronics & Molecular Engineering of Ministry of Education, Department of Chemistry, Tsinghua University, Beijing 100084, China
[c] Key Laboratory of Advanced Energy Materials Chemistry (Ministry of Education), Nankai University, Tianjin 300071, China

ARTICLE INFO

Article history:
Received 11 November 2025
Revised 26 December 2025
Accepted 30 December 2025
Available online 31 December 2025

Keywords:
Polyoxometalate
POM-based hybrid
Colorimetric sensor
Intelligent detection
Catalytic oxidation

ABSTRACT

Phenolic compounds are highly toxic environmental pollutants, posing significant risks to ecosystems and human health. Designing multifunctional catalysts capable of detecting, discriminating, and transforming these hazardous phenolics into valuable products represents a promising "waste-to-treasure" strategy. In this work, a novel Anderson-type polyoxometalate-based hybrid $[Ag(AlMo_6(OH)_6O_{18})]\cdot H_2L\cdot 2H_2O$ (**1**) (L = *N,N'*-bis(3-menthylpyridin-yl)naphthalene-2,6-dicarboxamide), was synthesized under solvothermal conditions. The assembly of $AlMo_6(OH)_6O_{18}^{3-}$ ($AlMo_6$) anion with Ag^+ ions formed a unique anionic inorganic [Ag-$AlMo_6$] nanosheet, further extended into a three-dimensional (3D) supramolecular by protonated H_2L^{2+} cations in an "S"-shaped arrangement. Compound **1** exhibits excellent peroxidase-like activity, enabling highly sensitive colorimetric detection of phenolic compounds with LODs ranging from 9.5 nmol/L to 63 nmol/L. Taking 2,3,6-TMP as a model analyte, smartphone-assisted visual detection was established with an LOD of 370 nmol/L. Moreover, a colorimetric sensor array combined with principal component analysis (PCA), successfully discriminated five structure similar phenolic compounds (2,3,6-trimethylphenol, 3,5-dimethylphenol, 2,3-dimethylphenol, *o*-chlorophenol, and *o*-bromophenol), demonstrating its potential for environmental monitoring. Beyond detection, compound **1** serves as an efficient heterogeneous catalyst for the selective oxidation of phenols to their corresponding quinones, achieving high conversion rates and selectivity. The catalytic mechanism and stability were systematically investigated using PXRD, the X-ray photoelectron spectroscopy (XPS), free radical trapping experiment, electron paramagnetic resonance (EPR) and Raman spectroscopy (RS). This work not only provides a robust platform for phenolic pollutant detection and discrimination but also advances the sustainable transformation of harmful waste into valuable chemical feed-stocks.

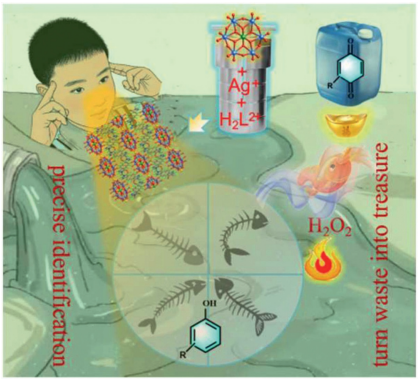
© 2026 Published by Elsevier B.V. on behalf of Chinese Chemical Society and Institute of Materia Medica, Chinese Academy of Medical Sciences.

Phenolic compounds, as a class of organic pollutants in natural environments and industrial products, exhibit significant ecotoxicity that poses severe threats to both environmental safety and human health [1–5]. It is of great significance to accurately identify them conveniently and turn "waste" into "treasure". Conventional detection methods (*e.g.*, electrochemical sensing, chromatography, electrochemiluminescence) are often limited by high costs, complicated operations and secondary pollution [6–10]. Meanwhile, traditional treatment technologies (*e.g.*, degradation, adsorption separation) fail to achieve resource recovery despite reducing pollution levels [11–15]. Consequently, developing integrated strategies combining high-sensitivity detection, accurate discrimination, and selective transformation of phenolic pollutants for "waste-to-treasure" conversion has become a crucial research direction in environmental remediation.

Polyoxometalate (POM)-based inorganic-organic hybrid materials demonstrate unique advantages in environmental catalysis due to their tunable electronic structures and abundant surface active sites [16–26]. These materials not only serve as efficient heterogeneous catalysts for organic transformations but also exhibit ideal biomimetic sensing properties owing to their distinctive redox characteristics [27–33]. For example, Lan's group confined POM clusters within the regular nanopores of a covalent organic framework *via* covalent bonds, forming a uniformly dispersed POM-based hybrid, which exhibited excellent performance in CO_2 photoreduction to CO [34]. Zheng *et al.* [35] reported a copper-

* Corresponding authors.
E-mail addresses: lgch1004@sina.com (G.-C. Liu), zhangzhong666@126.com (Z. Zhang), yonggewei@mail.tsinghua.edu.cn (Y.-G. Wei).

https://doi.org/10.1016/j.cclet.2025.112344
1001-8417/© 2026 Published by Elsevier B.V. on behalf of Chinese Chemical Society and Institute of Materia Medica, Chinese Academy of Medical Sciences.



Scheme 1. The schematic view of the catalytic synthesis of quinones from phenols and visual intelligent colorimetric identification of phenols using the title difunctional catalyst of **1**.

containing organic-inorganic polyniobate, which shows the highest catalytic activity for Knoevenagel condensation among the reported POMs. Song *et al*. [36] developed a novel iron-containing tungstate-based two-dimensional material for detecting oxidative stress biomarkers, with a detection limit of 58 nmol/L. Our team prepared six novel quinolinium-grafted polyoxometalates, which efficiently convert various benzyl alcohols into the corresponding benzoic acids using oxygen as the oxidant [37]. However, most existing POM-based materials focus on single functionalities, leaving three critical challenges unmet: (1) Portable and highly sensitive detection, (2) precise discrimination of structurally analogous compounds, and (3) highly selective catalytic conversion.

To address these challenges, we designed and synthesized a novel 3D supramolecular framework featuring a 2D Anderson-type POM-based nanosheet, namely $[Ag(AlMo_6(OH)_6O_{18})]\cdot H_2L\cdot 2H_2O$ (**1**, L = *N,N'*-bis(3-menthylpyridin-yl)naphthalene-2,6-dicarboxamide) under mixed-solvothermal conditions (Fig. S1 in Supporting information). The composition and structure of compound **1** were characterized by single crystal X-ray diffraction analysis, elemental analysis (EA), Fourier transform infrared spectroscopy (FT-IR), powder X-ray diffraction (PXRD), and X-ray photoelectron spectroscopy (XPS). The peroxidase-like activity of compound **1** was evaluated using hydrogen peroxide. Colorimetric detection and smartphone-assisted visual detection of phenolic compounds were performed with LODs at the "nm" level. A colorimetric sensor array by coupled principal component analysis (PCA) was established to accurately identify structurally related compounds, including 2,3,6-trimethylphenol (2,3,6-TMP), 3,5-dimethylphenol (3,5-DMP), 2,3-dimethylphenol (2,3-DMP), *o*-chlorophenol (2-CP), and *o*-bromophenol (2-BP). More remarkably, this title material serves as an efficient heterogeneous catalyst for the highly selective (>98 %) oxidation of 2,3,6-TMP into the value-added product TMBQ (2,3,5-trimethylbenzoquinone). Systematic investigations using multiple characterization techniques verified the catalyst's stability and reaction mechanism, demonstrating excellent recyclability. The proposed "detection-discrimination-transformation" integrated strategy establishes a new paradigm for combining environmental remediation with resource recovery, offering significant reference value for sustainable pollution control (Scheme 1).

0.030 g L ligand, 0.20 g $Na_3[AlMo_6(OH)_6O_{18}]\cdot 8H_2O$ and 0.08 g $AgNO_3$ were dissolved in a high-pressure reactor containing 7 mL deionized water and 3 mL ethanol mixed solution. The mixed solution was stirred for 2 h and heated at 120 °C for 4 days. After natural cooling, the gray-white crystals were obtained. The yield was 36 % based on Ag. Anal. calcd. for $C_{24}H_{26}AgAlMo_6N_4O_{28}$: C, 18.85; H, 1.71; N, 3.66. Found: C, 18.81; H, 1.83; N, 3.69. IR (KBr, cm^{-1}): 3627 (w), 3237 (w), 1634 (w), 1244 (w), 903 (s), 675 (s), 617 (s), 543 (w). The CCDC number of **1** is 2442736 (Table 1).

Table 1
Crystallographic data for compound **1**.

Compound	**1**
Formula	$C_{24}H_{26}AgAlMo_6N_4O_{28}$
Formula weight	1528.922
Crystal system	Monoclinic
Space group	*C*2/*c*
a (Å)	29.4142(13)
b (Å)	11.0254(4)
c (Å)	13.3412(5)
α/°	90
β/°	116.244(2)
γ/°	90
V (Å^3)	3880.6(3)
Z	4
D_c (g/cm^3)	2.617
μ (mm^{-1})	2.497
F (000)	2894.3
Reflection collected	64782
Data/restraints/parameters	3813/0/13
Goodness-of-fit on F^2	1.020
R [I≥2σ (I)]	$R_1 = 0.0216$, $wR_2 = 0.0544$
R [all data]	$R_1 = 0.0235$, $wR_2 = 0.0562$

$R_1 = \Sigma||F_o|-|F_c||/\Sigma|F_o|$, $wR_2 = \Sigma[w(F_o^2-F_c^2)^2]/\Sigma[w(F_o^2)^2]]^{1/2}$

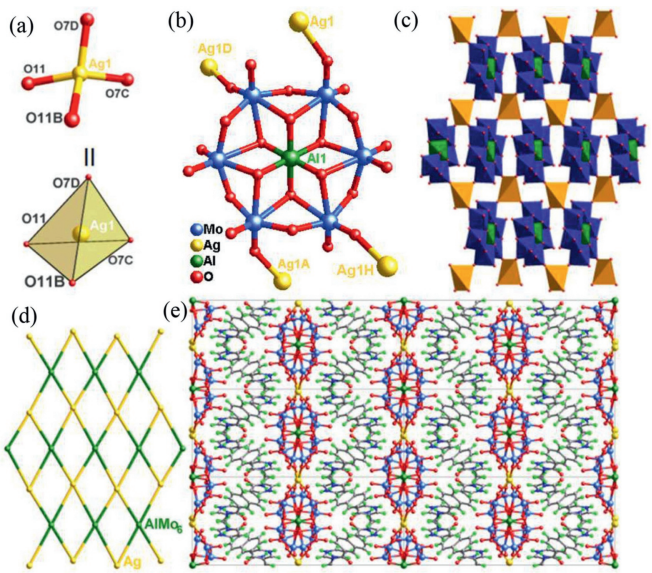


Fig. 1. The structure of **1**. (a) The coordinated environment of Ag^I. (b) The coordinated environment of $AlMo_6$ unit. (c) 2D inorganic network extended by 4-connected Ag and $AlMo_6$ units. (d) The schematic view of the 2D inorganic network. (e) The 3D supramolecular array containing 2D inorganic networks and H_2L^{2+} organic cations extended by H-bonds viewed along *c* axis filled with 2 × 3 cells.

Compound **1** is a three-dimensional supramolecular framework composed of an Ag-$AlMo_6$-based inorganic nano-anionic layer and protonated H_2L^{2+} cationic templates. The chemical valences of Ag, Mo, and Al calculated *via* the bond valence sum (BVS) are +1, +6 and +3, respectively (Table S1 in Supporting information). The structural unit consists of one Ag^+, one H_2L^{2+} organic cation, one $[AlMo(OH)_6O_{18}]^{3-}$ ({$AlMo_6$}) cluster and two crystalline water molecules. Each Ag^+ ion adopts a tetrahedral coordination geometry, bonding with four O atoms from four {$AlMo_6$} cluster (Ag1–O7C, 2.3187(3) Å, Ag1–O7D, 2.3187(3) Å, Ag1–O11, 2.2919(2) Å, Ag1–O11B, 2.2919(2) Å) (Fig. 1a and Table S2 in Supporting information). Meanwhile, each {$AlMo_6$} cluster connects four adjacent Ag^+ ions (Fig. 1b). Due to the paralleled stacking of the "cookie" shaped {$AlMo_6$} clusters, the 4-connected Ag^+ ions and

the 4-connected {$AlMo_6$} clusters assemble into a nanoscale inorganic anionic layer viewed along *b* axis (Figs. 1c and d). This layer has a thickness of approximately 1 nm. The inorganic layer exhibits a dumbbell-like morphology along the *b*-direction. To maintain charge balance, the protonated H_2L^{2+} exhibits adopt an "S"-shaped arrangement, serving as an organic cationic template (Fig. 1e). Thus, compound **1** ultimately exhibits a three-dimensional supramolecular framework extended by hydrogen bonds (Table S3 in Supporting information and Fig. 1e). To date, only a limited number of POM-based compounds incorporating Ag and {$AlMo_6$} unit have been reported. For example, Han *et al.* [38] successfully synthesized two POM-based compounds containing Ag, {$AlMo_6$} and H_2bpp ligand. Subsequently, Wang *et al.* [39] reported three additional POM-based compounds featuring Ag, {$AlMo_6$}, and 3-H_2pya ligands. Notably, compound **1** represents the first example of POM-based compound constructed from 2D Ag-$AlMo_6$-based inorganic layer and protonated H_2L^{2+} cationic ligand.

In the infrared spectrum of compound **1**, the absorption peaks in the range of 3100−3700 cm^{-1} correspond to the -CH_2 group in the N-containing ligand [40]. The absorption peak at 1600 cm^{-1} is attributed to the $\nu_{C=O}$ vibration absorption peak of the amide group in the organic ligand L [41]. The absorption peaks in the range of 1200−1600 cm^{-1} corresponds to the skeleton vibration of naphthalene ring. The peaks in the range of 640−780 cm^{-1} are the vibrational stretching caused by the $\nu_{C\text{-}N}$ of the *N*-heterocycle in the L ligand [42]. The 800−1000 cm^{-1} peaks are attributed to the stretching vibration of the characteristic peak in $[AlMo_6H_5O_{24}]^{4-}$ (Fig. S2a in Supporting information) [43]. The simulated and experimental powder X-ray diffraction (PXRD) patterns show that the diffraction peaks of the simulated and experimental PXRD patterns are basically consistent, which proves that compound **1** has good phase purity (Fig. S2b in Supporting information). The XPS spectrum of Ag ions in Fig. S2c (Supporting information) exhibits characteristic peaks at binding energies of 368.0 and 374.1 eV, which proves that the valence of Ag is + 1 [44]. Similarly, in Fig. S2d (Supporting information), the XPS spectra of Mo ions show characteristic peaks at binding energies of 232.6 and 235.8 eV, which are attributed to Mo(VI) ions [45].

To investigate the peroxidase-like properties of compound **1**, H_2O_2 was used as the oxidant and 2,3,6-TMP served as a representative substrate for the oxidative coupling reaction with 4-AAP (Fig. 2a). The formation of the pink coupling product, quinone imide (QI), was monitored by UV-vis absorption spectrum. As shown in Fig. 2b, when only H_2O_2 or compound **1** was added to the system containing 2,3,6-TMP and 4-AAP, no significant color change or enhanced UV-vis absorption peak near 500 nm was observed However, when H_2O_2 and compound **1** were present, obvious color changes were observed by the naked eye, and the solution changed from colorless to pink. This colorimetric response was corroborated by a significant enhancement of the UV-vis absorption peak near 500 nm. This confirms that compound **1** exhibits peroxidase-like activity, catalyzing the H_2O_2 mediated oxidation of 2,3,6-TMP and 4-AAP.

To explore the source of the peroxidase activity of compound **1**, control experiments were carried out under the same conditions using the individual precursors of compound **1**: L, $Na_3[AlMo_6(OH)_6O_{18}]\cdot 8H_2O$ or $AgNO_3$. Fig. 2c shows that L alone did not enhanced absorption peak near 500 nm, indicating no catalytic activity for the color reaction. When $Na_3[AlMo_6(OH)_6O_{18}]\cdot 8H_2O$ or $AgNO_3$ was used in this detecting systems, a strong absorption peak near 500 nm was observed, through they only exhibited weak catalytic activity for the color reaction. However, upon the introduction of compound **1**, the absorption peak of the system near 500 nm was enhanced most significantly. This enhancement effect was 7.6 times higher than that observed with $Na_3[AlMo_6(OH)_6O_{18}]\cdot 8H_2O$ and $AgNO_3$ alone. These

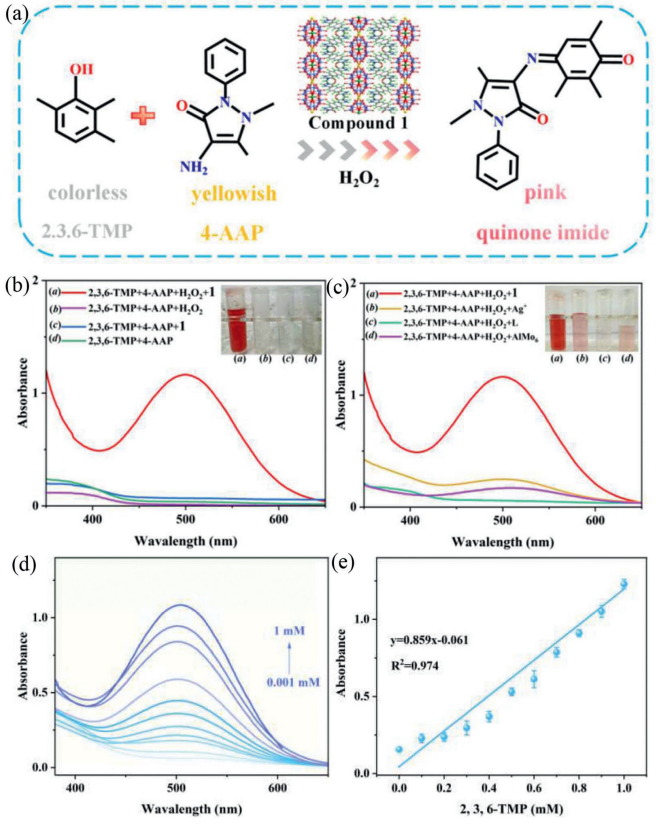


Fig. 2. (a) The schematic view of colorimetric sensing. (b) UV-vis absorption spectra of different systems. (c) UV-vis absorption spectra of different substances. (d) UV-vis absorbance spectra of the colorimetric detection of 2,3,6-TMP in the compound **1**+H_2O_2+4-AAP system. (e) The linear calibration curve for the detection of 2,3,6-TMP.

comparative experiments demonstrate that the peroxidase activity of compound **1** is attributed to the synergistic effect between $AgNO_3$ and $Na_3[AlMo_6(OH)_6O_{18}]\cdot 8H_2O$ within its structure.

To optimize the colorimetric detection performance of the 4-AAP+H_2O_2+**1** system, key parameters (pH, the dosages of 4-AAP, H_2O_2 and catalyst, reaction time) was evaluated using 2,3,6-TMP as a model substrate (Figs. S3a-e in Supporting information). As a result, 4-AAP: 1.5 mg/mL; pH: 6; H_2O_2: 6 mmol/L; catalyst: 0.6 mg/mL; reaction time: 30 min can be acted as the optimal conditions for the quantitative detection of phenolic compounds.

The system was tested with various phenolic compounds (2,3,6-TMP, 2,3-DMP, 2,6-DMP, 3,5-DMP, 2,3,5-TMP, 2.5-DMP, 2-MP) at concentration ranging from 0.001 mmol/L to 1 mmol/L. With the increase of the concentration of phenolic compounds (0.001−1 mmol/L), the absorbance at 500 nm gradually increased (Fig. 2d, Figs. S4 and S5a-f in Supporting information). In the concentration range of 0.001−1 mmol/L, the absorbance intensities have good linear relationships with the concentration of phenolic compounds (Fig. 2e and Figs. S6a-f in Supporting information). The detection limits of 2,3,5-trimethylphenol, 2,3-dimethylphenol, 2,5-dimethylphenol, 2,6-dimethylphenol, 3,5-trimethylphenol, *o*-cresol were 9.5, 17, 22, 18, 14, 18, 63 nmol/L, respectively. So far, metal elements, metal oxides and metal ions, *etc.* can be effectively combined with other substances to prepare composite materials for colorimetric detection phenols (Table S4 in Supporting information). Compared with the above previously published composites, the title compound **1** not only demonstrated comparable detection effect, but also has simple preparation process and low possibility of secondary pollution. Compared with most reported catalysts, compound **1** demonstrates superior detection sensitivity toward

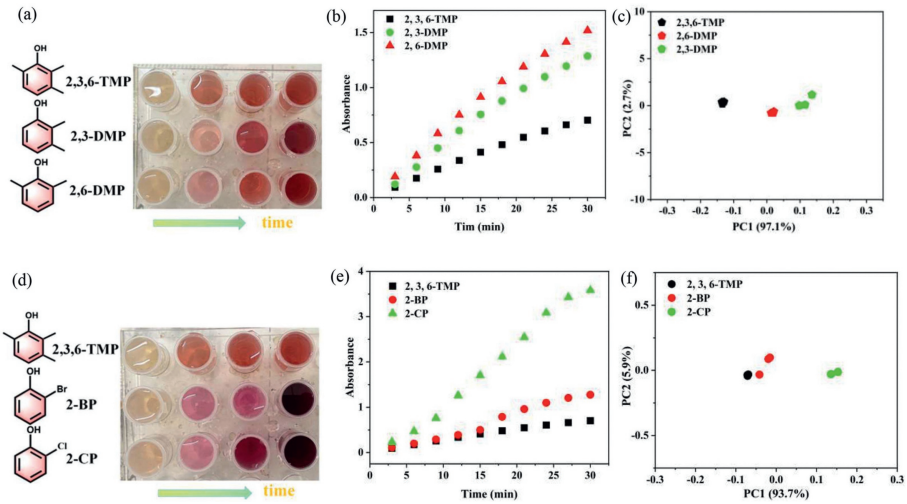


Fig. 3. (a, d) The structures of similar phenolic compounds and the corresponding change in color. (b, e) The absorbance intensity of the sensing system changed with time. (c, f) The PCA figures corresponding to the two groups phenols.

these phenolic compounds. To assess selectivity, potential interferents (acetone, ethanol, resorcinol, $NaNO_2$, 2-ethylimidazole, acetophenone, nitrobenzene, isobutyraldehyde, phloroglucionl) were introduced into the system. Their presence had negligible effects (Fig. S7 in Supporting information), confirming the high specificity and anti-interference capability of compound **1** for 2,3,6-TMP detection.

It is well known that hydroxyl radicals (·OH) are usually involved in the reactions catalyzed by POM-based or metal-oxide nanozymes [46,47]. Therefore, the fluorescence test was used for the ·OH-trapping experiment and the results revealed that all four groups of experiments exhibited an absorption peak at 425 nm, with the most intense signal observed in the presence of both H_2O_2 and compound **1** (Fig. S8 in Supporting information). According to previous reports, when H_2O_2 serves as the oxidant, POM-based nanozymes more readily produce ·OH radicals *via* multi-electron transfer and tunable redox potentials by catalyzing the homolytic cleavage of H_2O_2 [48]. In addition, when other transition metals (such as Ag) are incorporated into the POM-based structure, they can mimic Fenton-like reactions, thereby further enhancing the yield of ·OH [49]. In summary, the above analyses indicate that the peroxidase activity of **1** primarily arises from ·OH produced by H_2O_2 decomposition, which is consistent with the results of electron spin resonance (ESR) spectroscopy and the reported work (Fig. S9 in Supporting information) [50]. Due ·OH strong oxidative capacity, ·OH abstracts electrons from the hydroxyl group of phenol, forming quinone radicals. These radicals subsequently undergo oxidative coupling with 4-AAP to yield the pink-colored product (benzoquinone imine). These ·OH findings have been confirmed through radical trapping experiments and electron spin resonance (ESR) spectroscopy. In contrast, the catalytic mechanism of metal oxide-based nanozymes depends more strongly on their surface chemistry and variations in metal valence states.

Phenolic compounds exhibits varying degrees of environmental pollution, making their accurate discrimination a challenging yet critical research focus [51]. To explore the discrimination ability of compound **1** based on a colorimetric sensor, five phenols were divided into two research groups (Figs. 3a and d). Group I comprising 2,3,6-TMP, 2,6-DMP, and 2,3-DMP, have the same -CH_3 substituents but differ in their position and number. Group II consisting of 2,3,6-TMP, 2-CP, and 2-BP, have different types of substituents. As shown in Fig. 3, the time-dependent absorbance spectra of these two groups in the 4-AAP + H_2O_2 + **1** system reveal distinct reaction kinetics, as evidenced by different slopes (Figs. 3b and e). In group I, compared to 2,3,6-TMP and 2,3-DMP, 2,6-DMP exhibits a more sensitive color response in the sensing system (Figs. 3a and b). In group II, the sensitivity of the color response follows the order: 2-CP > 2-BP> 2,3,6-TMP (Figs. 3d and e). These findings enable the establishment of an effective sensing array based on the absorbance data of the two groups (Figs. 3c and f), which has the potential to effectively differentiate similar phenolic pollutants. The details of the array include 10 time points, 3 repetitions, and the data obtained are processed by principal component analysis (PCA) to generate a two-dimensional model diagram (Tables S5 and S6 in Supporting information) [52]. As shown in Figs. 3c and f, the three phenolic compounds in group I and the corresponding phenolic compounds in group II showed relatively independent distribution with small-scale dispersion, indicating the array's potential for complete identification of similar phenolic compounds [53,54].

Compared to large-scale instruments such as fluorescence spectrometers or UV-vis spectrometers, smartphone-based sensing platforms offer greater convenience, time-saving, and low-cost, making them widely used for portable sensing analysis. Therefore, we used a smartphone as the detection platform for 2,3,6-TMP. Different concentrations of 2,3,6-TMP were added to the 4-AAP+H_2O_2+**1** reaction system. After reacting for 30 min at room temperature, the solution turned from colorless to pink, a change visible to the naked eye. Subsequently, a smartphone was used to capture an image of the solution, and the R, G, B values were extracted (Fig. 4). The resulting calibration curve yielded a linear equation of $y = 1.419x + 1.394$ ($R^2 = 0.973$), with a LOD of 370 nmol/L (Fig. 4a and Table S7 in Supporting information). To validate the accuracy and reliability of the platform, TMB with concentrations of 0.3 and 0.7 mmol/L was added to the 4-AAP+ H_2O_2 + **1** reaction system. The measured R/B data values were 1.79 and 2,3,6-TMP, respectively. Calculating these values back using the linear equation yielded concentrations of 0.28 and 0.68 mmol/L, which showed excellent agreement with the actual spiked concentrations (Fig. 4b and Table S8 in Supporting information). These results confirm that the smartphone-assisted sensing platform can be used to monitor and analyze different concentrations of 2,3,6-TMP with good reliability.

p-Benzoquinone (*p*-BQ), a key intermediate for the synthesis of vitamin E, was the target product in this study. Therefore, the selective catalytic oxidation of 2,3,6-TMP to *p*-BQ was investigated using 2,3,6-TMP as the model substrate, 30% H_2O_2 as oxidant,

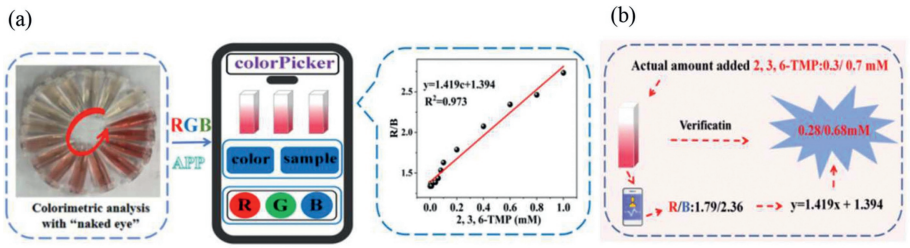
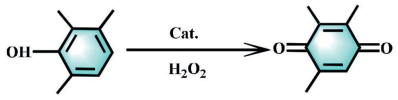


Fig. 4. (a) The schematic view of detection of 2,3,6-TMP using a smartphone. (b) The schematic view of quantitative analysis for 2,3,6-TMP.

Table 2
Synthesis of TMBQ from the oxidation of 2,3,6-TMP by **1**.[a]



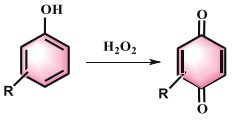
Entry	Cat. (mg)	H_2O_2 (mmol)	Conv. (%)	Sele. (%)[b]
1	6	0.75	77.60	94.0
2	8	0.75	80.8	92.0
3	10	0.75	98.0	98.0
4	12	0.75	88.1	>99
5	10	0.5	85.6	93.0
6	10	0.75	98.0	98.0
7	10	1	96.3	99.0
8	10	1.5	98.8	96.0
9	None	0.75	40.7	65.2
10	10	None	16.4	0

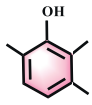
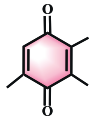
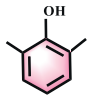
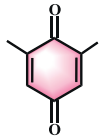
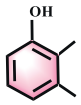
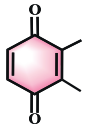
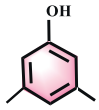
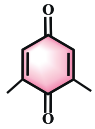
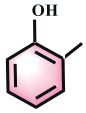
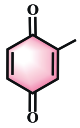
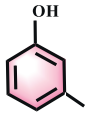
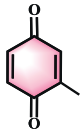
[a] Reaction conditions: 0.25 mmol of 2,3,6-TMP, 1.0 mL of ACN. Time: 15 min, Temp: 80 °C.
[b] Selectivity to TMBQ.

and compound **1** as a heterogeneous catalyst (Table 2). To optimize the reaction conditions, the effects of various parameters, including solvent, catalyst amount, reaction temperature, oxidant amount, and reaction time, were systematically studied. Firstly, the effects of different solvents on the reaction were studied. When ethanol, methanol, acetonitrile (ACN), dichloromethane and cyclohexane were used as solvents, the conversion rates were 71.7%, 66.4%, 73.7%, 39.5% and 96.5% (Fig. S10a and Table S9 in Supporting information). Secondly, the effect of catalyst on the reaction was also studied (Table 2, entries 1-4 and 9). As the mass of catalyst **1** increased from 0 mg to 12 mg, the conversion of 2,3,6-TMP rose from 40.7% to 98.0%, with selectivity increasing from 65.2% to 99.0%. The effect of the amount of oxidant on the reaction was further studied (Table 2, entries 5, 6, 7, 8, 10). Increasing the H_2O_2 amount from 0 mmol to 1.5 mmol, enhanced the conversion from 16.4% to 98.8%, with the selectivity improving from 0% to 99.0%. The selected temperature ranges of 60−90 °C, the conversion ranges from 71.9%−98.7%, and the selectivity ranges from 90.0%−98.0% (Fig. S10b and Table S10 in Supporting information). Finally, three reaction time periods (10, 15, 20 min) were considered to explore corresponding effect. The corresponding conversion rate is from 84.1% to 98.8%, and the selectivity is from 95.0% to 99.0% (Fig. S10c and Table S11 in Supporting information). Based on these results, the optimum reaction conditions were determined (acetonitrile as solvent, catalyst: 10 mg, H_2O_2: 0.75 mmol, reaction temperature: 80 °C, reaction time: 15 min). Under these optimal conditions, the reaction kinetics were studied. The plot of conversion versus reaction time showed a strong linear relationship, indicating that the reaction follows first-order kinetics with the rate constant (k) is 0.262 min^{-1} (Fig. S11 in Supporting information).

In order to study the multiple catalytic functions of compound **1**, the selective oxidation of various substituted phenol derivatives

Table 3
Catalytic oxidation of different substrates to *p*-BQs.[a]



Catal.	Substrate	Expected product	Conv. (%)	Sele. (%)[b]
1			95.5	91.0
2			85.5	99.0
3			64.5	45.0
4			56.0	65.2
5			68.4	85.7
6			54.1	76.3

[a] Reaction conditions: 0.25 mmol phenol; 10 mg compound **1**; 1.0 mL of ACN; temperature: 80 °C; Time: 15 min.
[b] Selectivity to TMBQ.

was conducted under the optimized conditions (Table 3). 2,3,5-Trimethylphenol (2,3,5-TMP), an isomer of 2,3,6-TMP (Table 3, entry 1), exhibited a lower conversion rate under the same conditions. This difference is mainly due to the large steric hindrance of 2,3,5-TMP at the para position, which limits the proximity of peroxopolyacid species in the oxygen transfer mechanism [55]. A similar trend was observed among the dimethylphenol isomers (2,6-dimethylphenol, 2,3-dimethylphenol, and 3,5-dimethylphenol). 2,6-Dimethylphenol, with the smallest steric hindrance around the reactive site, showed the highest conversion (85.5%), compared to 2,3-dimethylphenol (64.5%) and 3,5-dimethylphenol (56.0%) (Table 3, entries 2-4). Furthermore, *o*-cresol (68.4%) also demonstrated a higher conversion than *m*-cresol (54.1%), highlighting the influence

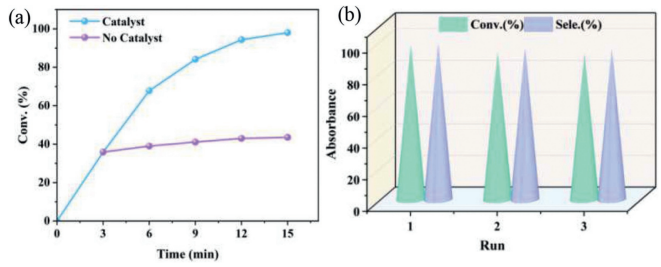


Fig. 5. (a) Hot filtration test for 2,3,6-TMP oxidation by compound **1** under optimal reaction conditions. (b) Recycle test for the oxidation of 2,3,6-TMP to TMBQ.

of the methyl group's position on the reaction activity (Table 3, entries 5 and 6) [56].

After 3 min of reaction, the solid catalyst in the reaction system was rapidly separated, and the filtrate was continuously heated. The results showed that the conversion rate remained almost unchanged, indicating that compound **1** acts as a heterogeneous catalyst (Fig. 5a). The stability and reusability of the catalyst were then evaluated. After the reaction, the solid catalyst was recovered, washed, and dried for subsequent analysis. The IR and PXRD of the recovered catalyst were nearly identical to those of the fresh sample (Figs. S2a and b), confirming its structural integrity. As shown in Figs. S12a and b (Supporting information), the XPS spectrum of Ag and Mo after the reaction exhibit characteristic peaks at binding energies of 368.15 and 374.20 eV for Ag, 232.81 and 235.62 eV for Mo [44,45], and these peaks are attributed to Ag^+ and Mo(VI). The XPS spectra confirm that the valence states of the atoms of **1** remain unchanged during the reaction. Furthermore, the catalyst was subjected to three consecutive recycling runs (Fig. 5b). No significant decrease in conversion or selectivity was observed, demonstrating that compound **1** possesses excellent reusability and stability.

To evaluate the role of compound **1** in the catalytic oxidation of 2,3,6-TMP, control experiments were performed. When $AgNO_3$ and L were used as catalysts, the conversions of 2,3,6-TMP were 19.2 % and 0 %, respectively (Table S12 in Supporting information, entries 1 and 2). Notably, using only $Na_3[AlMo_6(OH)_6O_{18}]\cdot 8H_2O$ as the catalyst gave a conversion of 54.2 % (Table S12, entry 3). Mixing the separate components of compound **1** to replace compound **1** also failed to fully oxidize the substrate (Table S12, entries 4 and 5), highlighting that the unique framework of compound **1** is essential for its high catalytic performance. Moreover, in the absence of catalyst or H_2O_2, the conversion of 2,3,6-TMP remained very low (Table 2, entries 9 and 10), indicating that both the catalyst and H_2O_2 are indispensable for efficient oxidation. Overall, the polyoxometalate (POM) contributes the main driving force for oxidation, while $AgNO_3$ plays a relatively minor role.

Although silver nitrate alone yields only a 19.2 % conversion, a weak radical involvement can still be inferred. Based on previous literature, the proposed mechanism can be deduced as follows [57,58]: Pathway A, in compound **1**, Ag^+ reacts with H_2O_2 to generate Ag^{2+}, ·OH and OH^-; the ·OH abstracts a hydrogen atom from the phenolic hydroxyl group, forming a phenoxy radical (**A1**) that undergoes intramolecular rearrangement (**A2**). Subsequently, Ag^{2+} reacts with H_2O_2, regenerating Ag^+ and producing ·OOH and H^+. The phenoxy radical (**A2**) then couples with ·OOH to afford the quinone product. To verify radical participation, control experiments were performed by adding 2,6-*di-tert*-butyl-*p*-cresol (BHT) as an oxygen-radical scavenger, 2,2,6,6-tetramethylpiperidine-*N*-oxide (TEMPO) as a carbon-radical scavenger, and isopropanol as an ·OH scavenger. The conversions remained at 84 %, 80.5 % and 89.2 % (Table S12, entries 6–8), further confirming the involvement of oxygen radicals and ·OH. Electron-paramagnetic-resonance (EPR) spectra of the reaction mixture displayed distinct radical signals (Figs. S13a and S9 in Supporting information). When $Na_3[AlMo_6(OH)_6O_{18}]\cdot 8H_2O$ is used alone, the conversion reaches 54.2 % (Table S12, entry 3), further confirming that the molybdenum-based polyoxometalate (POM) is the main driving force. Raman spectroscopy shows a characteristic band at 895 cm^{-1}, indicating the presence of an O–O bond (Fig. S13b in Supporting information) [59,60], which supports this mechanism. The proposed reaction pathway is as follows: Pathway B the POM cluster is first activated by H_2O_2 to generate an active peroxomolybdate species; this electrophilic species attacks the *para*-C–H bond of the substrate, forming intermediate **B1**, which rapidly converts to **B2**. **B2** is then further oxidized by another peroxomolybdate species, ultimately yielding the target product TMBQ (Fig. 6). In compound **1**, Ag^+ functions as an electron–transfer agent, generating ·OH radicals. POM can stabilize Ag species, prevent their agglomeration and deactivation, and may also regulate the oxidation state of Ag through their redox properties, thereby promoting the continuous generation of ·OH. Additionally, POMs can form peroxo-polyoxometalate active intermediates with H_2O_2, which are capable of directly oxidizing phenolic compounds.

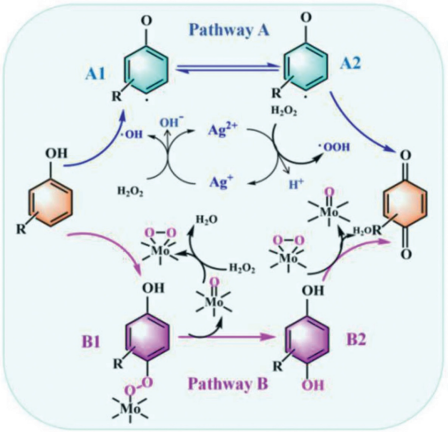


Fig. 6. The possible reaction mechanism.

In summary, we have successfully constructed, a new Anderson-type POM-based supramolecular framework $[Ag(AlMo_6(OH)_6O_{18})]\cdot H_2L\cdot 2H_2O$, by integrating anionic [Ag-$AlMo_6$] inorganic nanosheets with cationic amide-organic templates (H_2L^{2+}). This compound exhibits excellent peroxidase-like activity, enabling the rapid and ultrasensitive colorimetric detection of seven phenolic compounds with detection limits at the "nm" level. Based on the principal component analysis and smartphone-assisted sensing platform, the system utilizing compound **1** can not only can achieve the precise discrimination of five structurally similar phenols, but also enable rapid, portable and visual monitoring of organic phenolic pollutants. Beyond detection, compound **1** can catalyze the oxidation of various phenols to synthesize corresponding quinones, thus realizing the transformation from "waste" to "treasure". This work not only enables the rapid detection of organic pollutants but also facilitates the precise differentiation of structurally similar analogues, thereby providing a powerful tool for on-site environmental monitoring and analysis. This work provides valuable insights for environmental protection and pollutant management, highlighting the potential of POM-based materials in addressing pressing ecological challenges.

Declaration of competing interest

The authors declare that they have no known competing financial interests or personal relationships that could have appeared to influence the work reported in this paper.

CRediT authorship contribution statement

Lian Yang: Writing – original draft. **Guo-Cheng Liu:** Software. **Na Xu:** Validation. **Zhong Zhang:** Validation. **Xiu-Li Wang:** Funding acquisition. **Yong-Ge Wei:** Methodology.

Acknowledgments

This work was supported by the National Natural Science Foundation of China (NSFC, Nos. 22101030, 21901018, 22271021, 22571025), the Natural Science Foundation and Education Department of Liaoning province (Nos. LJ212410167017, LJ232410167011, LJ212510167020, 2025-MS-282, 2022-MS-373).

Supplementary materials

Supplementary material associated with this article can be found, in the online version, at doi:10.1016/j.cclet.2025.112344.

References

[1] S. Li, B.Q. Wang, G.C. Liu, et al., Inorg. Chem. Front. 11 (2024) 1561–1572.
[2] Y. Ding, C.H. Wang, L. Pei, et al., Inorg. Chem. Front. 10 (2023) 3756–3780.
[3] J. Yan, Q.H. Meng, X.J. Shen, et al., Sci. Adv. 6 (2020) eabd1951.
[4] C.Y. Zhu, B. Yang, Y. Zhao, et al., Polym. Chem. 4 (2013) 5395–5400.
[5] X.Z. Du, H.J. Fan, S.L. Liu, et al., Nat. Commun. 14 (2023) 4479.
[6] Z.N. Gu, Z.Y. Zhang, N. Ni, et al., Environ. Sci. Technol. 56 (2022) 4356–4366.
[7] S.U. Rehman, S.M. Babulal, H.F. Wu, et al., ACS Appl. Nano Mater. 7 (2024) 25004–25013.
[8] X. Liu, J.P. Guan, N.H. Zhou, et al., Inorg. Chem. 64 (2025) 13604–13610.
[9] L.H. Feng, K.J. Mao, X.Y. Zhu, et al., ACS Omega 10 (2025) 15553–15562.
[10] Y.Y. Wu, Y.Q. Li, H.J. Hu, et al., ACS EST Eng. 1 (2021) 603–611.
[11] Y. Chen, S.N. Sun, J.M. Lin, et al., Adv. Mater. 37 (2025) 2413638.
[12] H. Dong, L. Fang, K.X. Chen, et al., Angew. Chem. Int. Ed. 64 (2025) e202414287.
[13] Z.C. Zhao, J.Y. Wei, Z.L. Lang, et al., J. Am. Chem. Soc. 147 (2025) 25107–25114.
[14] J. Li, P.P. Shao, W.J. Geng, et al., Green Chem. 27 (2025) 827–837.
[15] S.Z. Chang, H.Y. An, Y.H. Chen, et al., ACS Sustain. Chem. Eng. 10 (2022) 4728–4740.
[16] X.Y. Zhang, N. Xu, Z.H. Shang, et al., Inorg. Chem. 64 (2025) 6137–6141.
[17] W.M. Huang, Q.S. Yang, W.M. Chen, et al., J. Am. Chem. Soc. 174 (2025) 5572–5576.
[18] Y. Chen, A.G. Liu, Z.T. Chen, et al., ACS Catal. 14 (2024) 16605–16617.
[19] A.V. Anyushin, A. Kondinski, T.N. Parac, et al., Chem. Soc. Rev. 49 (2020) 382–432.
[20] W.H. Zhang, Q.F. Luo, L. Sheng, et al., JACS Au 12 (2021) 2130–2145.
[21] X.J. Zheng, Q.Z. Zhu, H.Q. Song, et al., ACS Appl. Mater. Interfaces 7 (2015) 3480–3491.
[22] Y. Zheng, Z. Zhang, N. Xu, Tungsten (2025), doi:10.1007/s42864-025-00365-6.
[23] X.Y. Ma, H.X. Bi, X.J. Zhang, et al., Polyoxometalates 5 (2025) 9140090.
[24] H. Song, M.S. Guo, J.F. Wang, et al., Polyoxometalates 4 (2024) 9140065.
[25] F. Abbas, S.H. Talib, S. Mohamed, et al., J. Phys. J. Mater. Chem. C 129 (2025) 13203–13218.
[26] F. Abbas, Y.G. Wei, et al., Int. J. Hydrog. Energy 117 (2025) 1–11.
[27] Y. Zheng, J.Y. Sun, Z. Zhang, et al., J. Mol. Struct. 1337 (2025) 142176.
[28] J.C. Liu, J.F. Wang, Q. Han, et al., Angew. Chem. Int. Ed. 60 (2021) 1153–1157.
[29] Q.L. Liu, X. Wang, et al., Angew. Chem. Int. Ed. 62 (2023) e202217764.
[30] H.P. Xiao, Y.S. Ha, X.X. Li, et al., Angew. Chem. Int. Ed. 61 (2022) e202210019.
[31] J.C. Liu, J.W. Zhao, C. Streb, et al., Coord. Chem. Rev. 471 (2022) 214734.
[32] D. Wang, J. Jiang, M.Y. Cao, et al., Nano Res. 15 (2022) 3628–3637.
[33] J.C. Liu, Q. Han, L.J. Chen, et al., Angew. Chem. Int. Ed. 57 (2018) 8416–8420.
[34] M. Lu, M. Zhang, J. Liu, et al., J. Am. Chem. Soc. 144 (2022) 1861–1871.
[35] Y.K. Zuo, Y.R. Li, Y.Q. Sun, et al., Inorg. Chem. Front. 11 (2024) 1993–1997.
[36] J. Jiang, Y.Z. Li, L.L. Liu, et al., ACS Appl. Mater. 15 (2023) 1486–1494.
[37] S. Ru, C.C. Zhao, Z.K. Wu, et al., ACS Sustain. Chem. Eng. 12 (2024) 6827–6839.
[38] J.S. Yan, K.N. Gong, X.L. Xue, et al., Eur. J. Inorg. Chem. 34 (2014) 5969–5976.
[39] H.M. Zeng, B.X. Jin, W.H. Wu, et al., Chem. Mater. 34 (2022) 2989–2997.
[40] G.B. Li, J. Chen, B.Q. Song, et al., ACS Appl. Mater. 36 (2025) 50916–50924.
[41] Y.M. Cui, Y.J. Zhu, J. Sun, et al., ACS Mater. Lett. 6 (2024) 4255–4261.
[42] X.M. Luo, N.F. Li, Z.B. Hu, et al., Inorg. Chem. 58 (2019) 2463–2470.
[43] B.Y. Zhang, N.H. Wang, X.S. Wu, et al., Inorg. Chem. 64 (2025) 19933–19938.
[44] N. Khalaf, T. Ahamad, M. Naushad, et al., Int. J. Biol. Macromol. 46 (2020) 763–772.
[45] J. Cao, J. Yun, N. Zhang, et al., Synth. Met. 282 (2021) 116931.
[46] J. Ma, X.H. Li, N. Xu, J. Catal. 452 (2025) 116444.
[47] J.J. Xina, H.J. Pang, S.U. Khan, et al., Appl. Surf. Sci. 619 (2023) 156713.
[48] D. Chang, Y.D. Li, Y.X. Chen, et al., Nanoscale Adv. 4 (2022) 3689.
[49] M.H. Zhang, Y.X. Zhou, B.Y. Wu, et al., Mater. Adv. 4 (2023) 5420.
[50] X. Bai, M.C. Zhu, Y.F. Liu, et al., Mater. Today Chem. 48 (2025) 102929.
[51] J.J. Xin, H.J. Pang, Z.X. Jin, et al., Inorg. Chem. 61 (202) 16055-16063.
[52] L. He, Y. Yang, X.X. Wang, et al., Anal. Chim. Acta 1384 (2026) 344941.
[53] Z.Y. Gao, J.P. Guan, M. Wang, et al., Talanta 272 (2024) 125840.
[54] J.J. Xin, H.J. Pang, Z.X. Jin, et al., Inorg. Chem. 61 (2022) 16055–16063.
[55] S.Z. Chang, H.Y. An, Y.H. Chen, et al., ACS Sustain. Chem. Eng. 10 (2022) 4728–4740.
[56] S.Z. Chang, Y.H. Chen, H.Y. An, et al., ACS Appl. Mater. Interfaces 13 (2021) 21261–21271.
[57] M.H. Zhang, Y.X. Zhou, B.Y. Wu, et al., Mater. Adv. 4 (2023) 5420.
[58] S.Z. Chang, H.Y. An, Y.H. Chen, et al., ACS Sustain. Chem. Eng. 10 (2022) 4728–4740.
[59] Y. Sun, Z. Zhang, N. Xu, et al., J. Mater. Chem. A 13 (2025) 42402.
[60] Y. Wang, W.S. Fang, D.Y. Zhub, et al., Prog. Mater. Sci. 157 (2026) 101594.